

3D numerical analysis of magnetic topology and edge transport for RMP limiter scenarios at TEXTOR and DIII-D

H.G. Frerichs¹, O. Schmitz¹, D. Harting¹, D. Reiter¹, B. Unterberg¹, Y. Feng², T.E. Evans³, M.E. Fenstermacher⁴, I. Joseph⁵, R.A. Moyer⁵

¹ Institut für Energieforschung - Plasmaphysik, Forschungszentrum Jülich GmbH, Germany

² Max Planck Institut für Plasmaphysik, IPP-EURATOM Association, Greifswald, Germany

³ General Atomics, San Diego, California, CA 92186, USA

⁴ Lawrence Livermore National Laboratory, P.O. Box 808, Livermore, CA 94550, USA

⁵ University of California, San Diego, LA Jolla, CA 92093, USA

Introduction

Resonant magnetic perturbations (RMPs) are applied in the tokamaks TEXTOR, DIII-D and JET in order to control particle and heat flux in the plasma edge layer. This allows mitigation or complete suppression of edge localized modes (ELMs), an instability intrinsic to H-mode plasmas [1, 2]. However, the application of RMPs induces an open chaotic system at the plasma edge, leading to a complex 3D magnetic field structure. To investigate the resulting impact on plasma and neutral transport the 3D edge transport code EMC3-EIRENE [3, 4, 5] has been adapted to conditions of TEXTOR under the influence of the Dynamic Ergodic Divertor (DED) [6, 7]. Reasonable agreement to experimental data [8, 9] has been achieved and the code is now for the first time also used for DIII-D limiter scenarios. In this paper similar plasma scenarios at both machines are presented and compared, each showing a poloidal localized increase in outward transport. Modeling of the heat and particle flux footprints in DIII-D limiter plasmas suggests a strong influence of cross-field diffusion for typical L-mode transport coefficients.

RMP scenarios at TEXTOR-DED

At TEXTOR-DED a specific plasma setup was developed showing a DIII-D similar perturbed magnetic topology. This facilitates direct comparisons and code benchmarks. In this setup the plasma is shifted outwards, towards the ALT-II limiter. Here, magnetic lobes with field lines of long connection length L_c penetrate into the regular SOL region up to $\psi_N = 1.06$ (figure 1), with ψ_N being the normalized poloidal flux. These lobes extend the confined plasma region at certain poloidal locations (shaded box in figure 1) but also increase the local outward transport by transport along field lines. 3D plasma transport calculations with EMC3-EIRENE show an increase of electron density n_e and temperature T_e in the outward reaching lobes L_o ($\psi_N = 1.06$) compared to a reference position R_o :

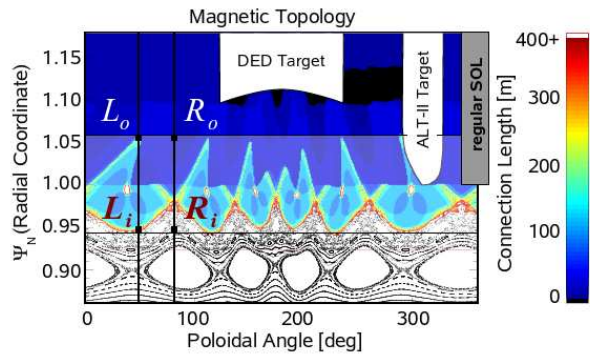


Figure 1: Magnetic topology in toroidal plane $\phi = 0^\circ$ for an $m/n = 6/2$ RMP scenario at TEXTOR with outward shifted plasma. The connection length L_c is depicted by color code, while intersections of field lines with the toroidal plane $\phi = 0^\circ$ are marked by black dots.

$$\frac{n_e(L_o)}{n_e(R_o)} = 3.4 \quad , \quad \frac{T_e(L_o)}{T_e(R_o)} = 1.8 \quad ,$$

while at the corresponding inner locations L_i, R_i ($\psi_N = 0.95$) n_e and T_e are reduced:

$$\frac{n_e(L_i)}{n_e(R_i)} = 0.82 \quad , \quad \frac{T_e(L_i)}{T_e(R_i)} = 0.84 \quad .$$

Thus, the formation of outward reaching lobes increases the effective outward transport. This is also evident from a flattening of the n_e and T_e profiles (figure 2), depicted by mean radial gradients at the poloidal positions L compared to R (normalized at the inner position):

$$\frac{\nabla n_e^*(L)}{\nabla n_e^*(R)} = 0.82 \quad , \quad \frac{\nabla T_e^*(L)}{\nabla T_e^*(R)} = 0.44 \quad , \quad (1)$$

$$\text{where} \quad \nabla f^* \equiv \frac{\Delta f}{\Delta \psi_N f_i} \quad .$$

From there, diffusion into the regular SOL affects transport to the target plates, leading to blurred strike points at the corners of the ALT-II limiter. (Compare magnetic and particle flux footprint in figure 3.)

The RMP limiter scenario at DIII-D

As RMPs with similar toroidal mode numbers ($n = 1, 2, 3$) are also applied at the DIII-D tokamak, an investigation of DIII-D limiter plasmas in comparison to TEXTOR findings provides further insights into the effect of RMPs on plasma transport. We choose a limiter plasma with an $n = 3$ perturbation from the I-coils in even parity, neglecting the additional error field and the $n = 1$ error field correction by the C-coils.

The plasma is limited by the inner wall on the HFS, thus creating a plasma wetted area on the wall around the midplane. The application of $n = 3$ RMPs leads to a strongly stochastic edge plasma up to $\psi_N = 0.85$ (figure 4). Lobes of stochastic field lines penetrate into the regular SOL, similar to the TEXTOR scenario shown above, but here only up to $\psi_N = 1.016$. In between field lines of short L_c form so called laminar flux tubes that open the boundary region (dark blue regions inside the shaded

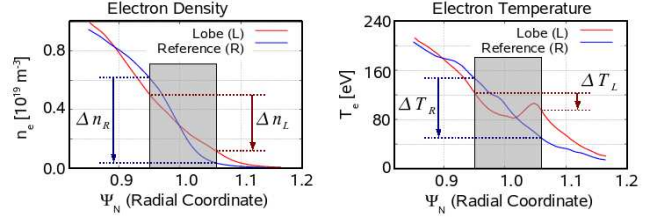


Figure 2: Radial profiles of n_e and T_e from transport modeling with EMC3-EIRENE. The gray shaded bars mark the radial region with lobes (compare to figure 1).

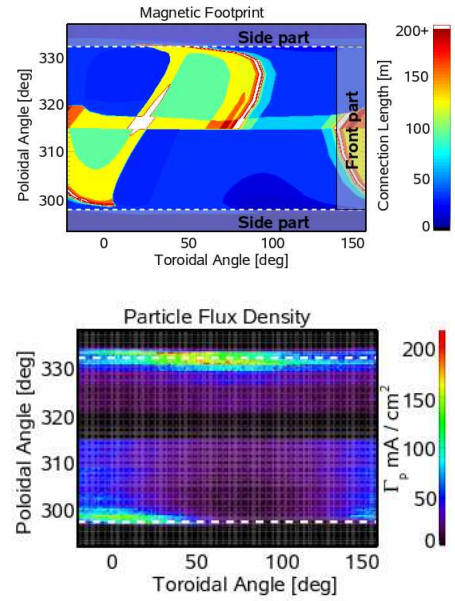


Figure 3: Magnetic footprint and particle flux footprint on ALT-II limiter from transport modeling with EMC3-EIRENE.

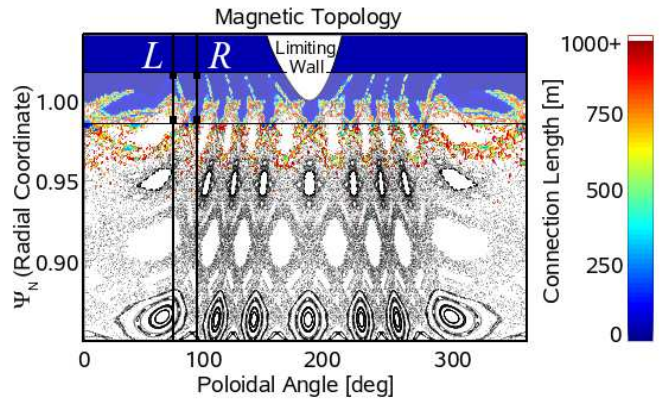


Figure 4: Magnetic topology in toroidal plane $\phi = 0^\circ$ for a DIII-D limiter plasma with $n = 3$ RMP field.

called laminar flux tubes that open the boundary region (dark blue regions inside the shaded

box in figure 4). Note, however, that the poloidal extent of magnetic structures is smaller due to the higher base mode number of the perturbation field with respect to the TEXTOR scenario shown above. 3D transport calculations with EMC3-EIRENE show a clear modulation of n_e and T_e (figure 5) according to the underlying magnetic topology (compare to figure 4). Again a reduction of normalized mean gradients is found at poloidal location with outward reaching lobes (L, figure 4), indicating an increase in outward transport:

$$\frac{\nabla n_e^*(L)}{\nabla n_e^*(R)} = 0.84, \quad \frac{\nabla T_e^*(L)}{\nabla T_e^*(R)} = 0.54. \quad (2)$$

These values are similar to the TEXTOR calculations in equation 1.

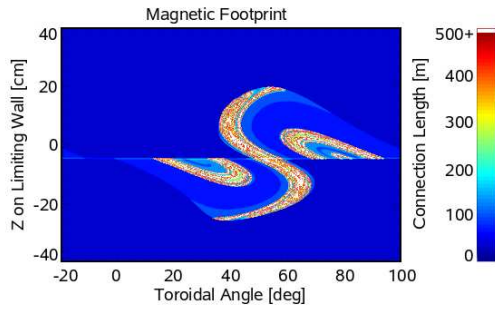


Figure 6: Magnetic footprint of an $n = 3$ limiter scenario at DIII-D.

Thus, the width of the lobe structure $\Delta\varphi \approx 10^\circ$, that is $\Delta L \approx 18$ cm, is by an order of magnitude larger than typical widths of lobe structures in poloidal divertor scenarios at DIII-D [10]. Therefore, this limiter scenario is optimal for resolving possible substructures inside lobes for direct diagnosis of the stochastic layer width.

However, for the perpendicular transport coefficients $D_\perp = 0.9 \text{ m}^2 \text{ s}^{-1}$ and $\chi_\perp = 3.6 \text{ m}^2 \text{ s}^{-1}$ used for the modeling shown in figure 5, transport towards the wall is significantly affected by cross-field diffusion and no clear structures are visible (figure 8 top left). The predicted particle flux density Γ_p in the regular SOL is about 60% of Γ_p in the strike point region.

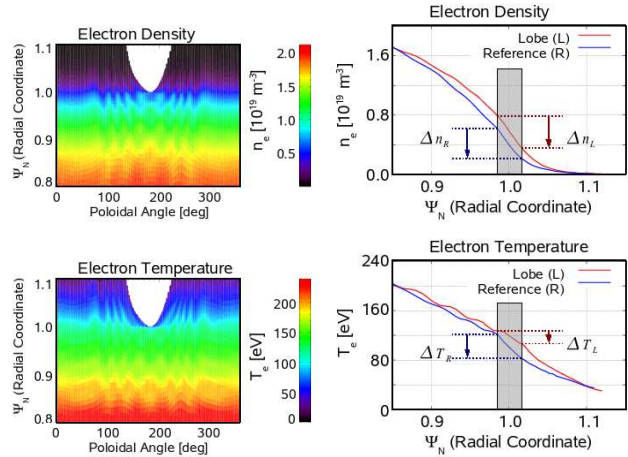


Figure 5: 2D profiles of n_e and T_e in toroidal plane $\varphi = 0^\circ$ (top) and radial profiles (bottom), both from transport modeling with EMC3-EIRENE.

We now focus on the last step of outward transport, i.e. how particles (and heat) are deposited on the limiting wall. The magnetic footprint (figure 6) shows a distinct toroidal localization of hitpoints from field line with long L_c , i.e. field lines coming from inside the plasma domain and open laminar flux tubes in between. The S-shaped part of the strike point is formed by a helical rotation of lobes of open field lines, touching the wall at a shallow incident angle (figure 7).

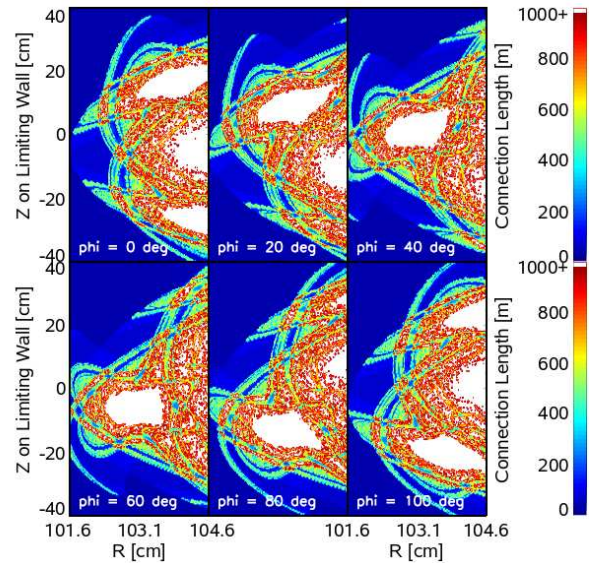


Figure 7: Toroidal evolution of lobes in front of the limiting wall forming an S-shaped strike point with two side parts at distinct sided of the midplane.

A reduction of D_{\perp} and χ_{\perp} by one order of magnitude leads to a clear toroidal localization of Γ_p in accordance with the boundary of the strike point. Inside the strike point a great amount of particle flux comes from the domain with short L_c , i.e. the laminar flux tubes. Another reduction of D_{\perp} and χ_{\perp} by one order of magnitude leads to a sharp alignment of Γ_p to the magnetic topology. A peaking of Γ_p is observed inside lobe strike points while Γ_p is reduced to 25% inside laminar flux tubes. If these patterns in particle and heat flux can be observed in experiment, detailed comparisons to modeling results could be made to estimate maximum values for D_{\perp} and χ_{\perp} .

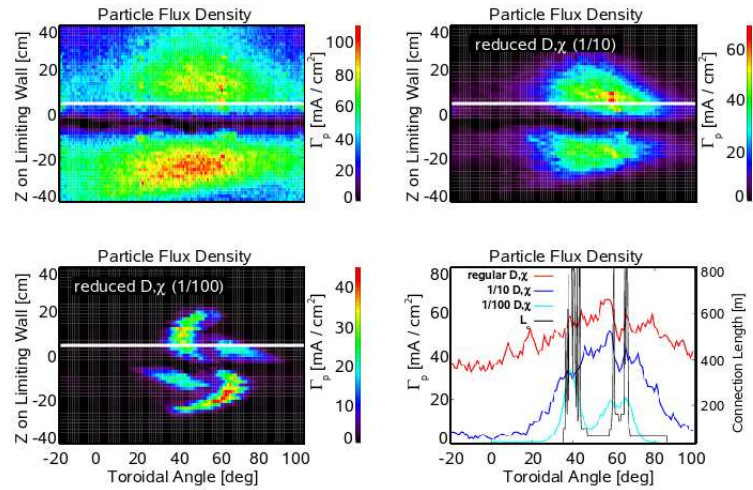


Figure 8: Particle flux footprints for $D_{\perp} = 0.9 \text{ m}^2 \text{ s}^{-1}$ and $\chi_{\perp} = 3.6 \text{ m}^2 \text{ s}^{-1}$ (top left), $1/10 D_{\perp}, \chi_{\perp}$ (top right), $1/100 D_{\perp}, \chi_{\perp}$ (bottom left) and as toroidal profiles at $Z = 5 \text{ cm}$ (bottom right), all from transport modeling with EMC3-EIRENE.

Conclusions

Specific RMP scenarios at TEXTOR and limiter RMP scenarios at DIII-D show comparable magnetic topologies and transport characteristics. Magnetic lobes entering the regular SOL increase local outward transport, leading to a localized reduction of radial gradients and to a poloidal modulation of plasma parameters in the regular SOL. For typical L-mode transport coefficients D_{\perp} and χ_{\perp} , the structures of particle and heat flux footprints are significantly affected by cross-field diffusion and do not reflect the detailed structure of the magnetic footprint. Thus, only in H-mode plasmas with reduced D_{\perp} , χ_{\perp} observation of magnetic structures in particle- and heat flux footprints is expected in DIII-D. These findings allow for the design of dedicated experiments to diagnose the stochastic layer and can provide an estimate for an upper limit of D_{\perp} and χ_{\perp} .

Work supported in part by the US Department of Energy under DE-FC02-04ER54698, DE-AC52-07NA27344, and DE-FG02-07ER54917.

References

- [1] T.E. Evans et al, *Phys. Rev. Lett.* **92**, 235003 (2004)
- [2] Y. Liang et al, *Phys. Rev. Lett.* **98**, 265004 (2007)
- [3] Y. Feng et al, *J. Nucl. Mater.* **241-243**, 930 (1997)
- [4] Y. Feng et al, *Contrib. Plasma Phys.* **44**, 1-3, 57 (2004)
- [5] D. Reiter et al, *Fusion Science and Technology* **47**, 172 (2005)
- [6] M. Kobayashi et al, *Contrib. Plasma Phys.* **44** 1-3, 25 (2004)
- [7] M. Kobayashi et al, *Nucl. Fusion* **44** S64 (2004)
- [8] O. Schmitz et al, *J. Nucl. Mater.* **363-365**, 680 (2007)
- [9] O. Schmitz et al, *Nucl. Fusion* **48** 024009 (2008)
- [10] A. Wingen et al, submitted to *Phys. Plasmas* (2008)